International Journal of Engineering and Geosciences
https://dergipark.org.tr/en/pub/ijeg
e-ISSN 2548-0960

Detection of irrigated crops using Landsat 8 images: A methodology based on fieldwork and spectral reflectance analysis

Abdelaziz El-Bouhali*[1], Mhamed Amyay[1], Khadija El Ouazani Ech-Chahdi[1]

[1] Ibn Zohr University, Department of Geography - FLASH Ait Melloul, Morocco, a.elbouhali@uiz.ac.ma
[2] Sidi Mohamed Ben Abdellah University, Department of Geography – FLSH Sais Fez, Morocco, mhamedamyay@hotmail.com, khadija.elouazaniechachahdi@usmba.ac.ma

Cite this study: El-Bouhali, A., Amyay, M., & El Ouazani Ech-Chahdi, K. (2025). Detection of irrigated crops using Landsat 8 images: A methodology based on fieldwork and spectral reflectance analysis. International Journal of Engineering and Geosciences, 10 (1), 1-13.

https://doi.org/10.26833/ijeg.1483206

Keywords
Remote sensing
Fieldwork
Spectral reflectance
Irrigated crops
Guigou depression

Research Article

Received: 13.05.2024
Revised: 09.08.2024
Accepted: 27.08.2024
Published:01.02.2025

Abstract

The mapping and quantification of agricultural surfaces using remote sensing (RS) data at different scales and environmental conditions have become essential to ensure the implementation of a sustainable water resource management policy. On a global scale, the steady increase in publications over the last decades reflects the significance of optical satellite images in studying land use (LU). In the present study, we suggest a methodology to identify the most suitable dates and spectral bands for mapping irrigated crops in the Guigou depression. The methodology relies primarily on fieldwork and spectral reflectance (SR) analysis. The extraction of irrigated crops is carried out using the Support Vector Machine (SVM) classification algorithm. The integration of SR data and fieldwork has indicated that August is the most favorable month for studying irrigated crops. Thus, it was concluded that the Near Infrared band is the most effective for discriminating agricultural surfaces. Results from processing Landsat 8 satellite images (L8SI) reveal that classification accuracy varies depending on land use (LU) classes. The mapping of major LU classes indicates a high level of agreement between the classified image and ground truth, with an accuracy of 0.97 (97%). The crop types classification (irrigated crops) shows low accuracy for potatoes and carrots, with an F1 Score, User's Accuracy, and a Producer's Accuracy below 0.8. Based on the classification accuracy level, we observed that the combination of SR, fieldwork, and legend selection criteria has a high potential for distinguishing irrigated crops from other LU classes. The approach developed in this work has highlighted the importance of Landsat OLI images in mapping and quantifying agricultural surfaces in the GD. This approach could be valuable in other regions to select periods favorable to the study of irrigated crops.

1. Introduction

Optical remote sensing (RS) provides pertinent and efficient data for monitoring land surface dynamics across diverse environmental conditions [1,2] at global and continental scales [3-6]. Open access to satellite data archives and the availability of satellite images have contributed to the development of various supervised classification algorithms that allow for extracting information from raw images. These algorithms, widely used in the literature [7-9], have been applied to various types of satellite images (Landsat, MODIS, and Sentinel-2) for mapping land use (LU). In parallel with supervised classification methods, authors have used optical indices derived from satellite images, such as the Normalized Difference Vegetation Index (NDVI), the Soil Adjusted Vegetation Index (SAVI), and the Enhanced Vegetation Index (EVI) to distinguish irrigated crops and other LU classes under diverse environmental conditions and at varying scales [10-16].

The availability of satellite images provided by space agencies (National Aeronautics and Space Administration: NASA, European Space Agency: ESA, etc.) and the development of tools and image processing algorithms have led to an ongoing increase in publications based on multi-source and multi-date image processing [17-24]. While Landsat images are considered among the most used in the field of remote sensing [25], the launch of Sentinel-2 satellite images with high spatial resolution (10 m) and temporal

resolution (every five days) has provided a feasible solution and opened new opportunities for monitoring agricultural lands [26] and LU dynamics. In this context, [27] has demonstrated that spatial RS data has become indispensable for monitoring ecosystems at both global and local scales. The increasing number of studies focusing on LU studies illustrates this finding [28-31]. Currently, mapping LU from satellite images is a significant component of scientific research. Moreover, the Global Climate Observing System program (GCOS) classifies this theme among essential climate variables [32].

The results obtained across various environmental conditions and spatiotemporal scales demonstrate the effectiveness of satellite data and image processing methods. Furthermore, studies related to LU suggest a notable increase in agricultural land at the expense of forests and natural meadows [33,34]. These modifications in land surfaces contribute to environmental degradation and the intensification of hydrological deficits. This issue is expected to worsen with climate change and the increasing demand for irrigation water in the coming years. In this context, the FAO (Food and Agriculture Organization) estimates that 80% of food requirements in 2025 will be covered by irrigated agriculture [35,36]. Given this situation, mapping and quantifying irrigated agricultural surfaces from satellite images at various scales have become significant challenges, as these images form the foundation for establishing a sustainable water resource management policy. However, extracting information related to irrigated surfaces and crops from satellite images requires the implementation of a robust methodology. In this context, the current study aims to map irrigated crops within the Guigou depression (GD). Specifically, the main objectives of this research are: 1) identifying the favorable period for distinguishing irrigated crops from other LU classes based on fieldwork and SR analysis. 2) Spatialisation and quantification of irrigated crops from Landsat 8 satellite imagery using the Support Vector Machine (SVM) classification algorithm.

2. Materials and methods

2.1. Study area

The GD (Figure 1) is situated in the Tabular Middle Atlas (TMA). It extends within the upper Sebou watershed, covering an area of approximately 190 km^2. Faulted limestone formations overlaid with basaltic flows dominate the study area [37]. This hydrogeological context is conducive to water infiltration and the presence of underground aquifers. The soils exhibit varying depths depending on the locations. At the bottom of the depression, soils resulting from slope erosion are relatively deep, while at the margins, the soils are shallower. Surface runoff is rare and mainly linked to karstic springs [38]. The elevations range from 1495 meters at the urban center of Guigou to 2310 meters at the North Middle Atlas Accident. The climate is semi-arid, characterized by a dry summer and a rainy or snowy winter.

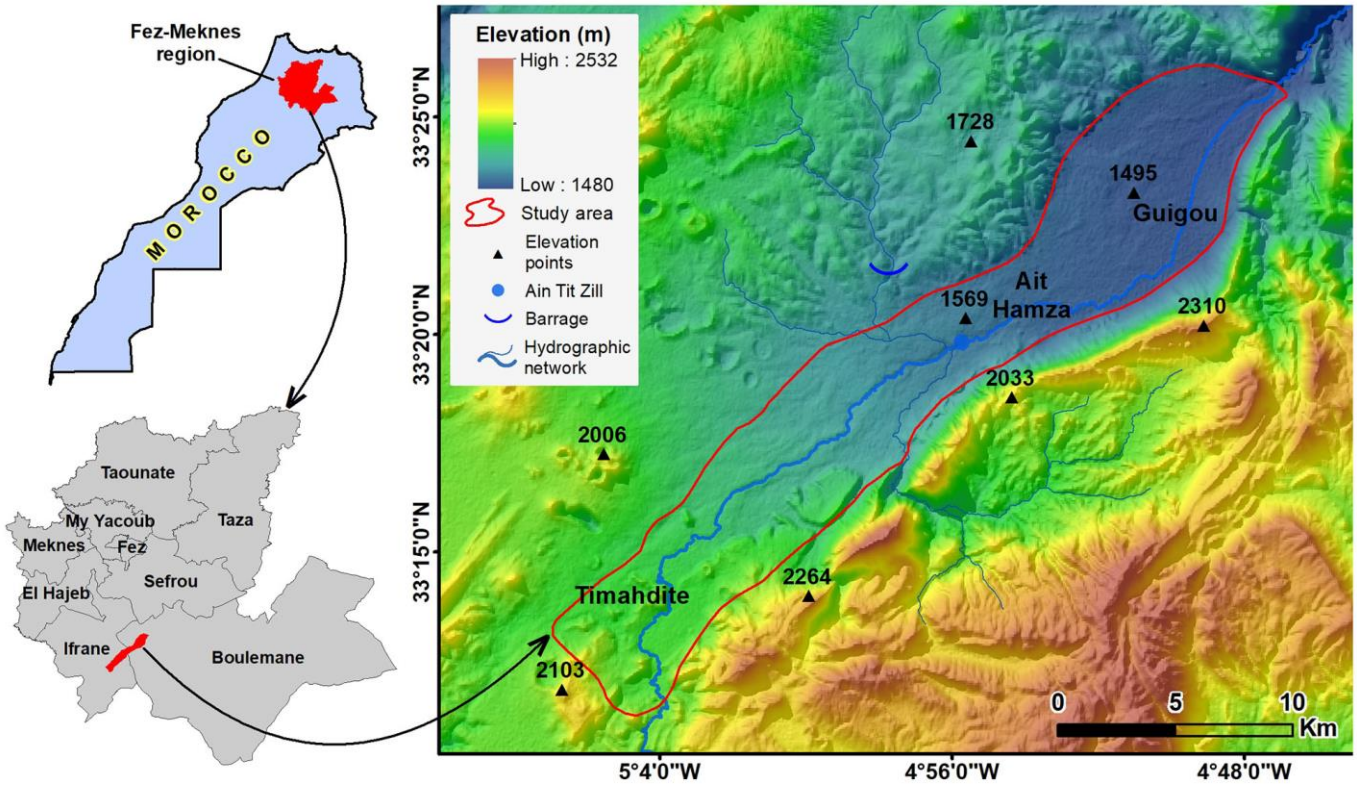

Figure 1. Study area location map

Situated within the TMA, the GD was a grazing land where transhumance was practiced by local herders and neighboring regions [39,40]. Economic activity was centered around transhumant livestock, with a limited area dedicated to rainfed and irrigated crops. The irrigation of the fluvial terraces along the wadis and downstream of springs was carried out through a traditional network derived from the Guigou wadi and its

sources [41]. With population growth, state interventions, and consecutive dry years, this area has undergone significant transformations over the last decades. It is primarily marked by an extension of irrigated crops (potatoes, onions, carrots, etc.) to the detriment of rainfed agricultural land and pasturelands [42-44].

The agricultural parcels in the GD vary in size. The classification of parcels based on their size (Figure 2) reveals a significant predominance of small-sized parcels [≤ 1 and between 1 and 2 hectares], which represent approximately 72% of the study area. Medium-sized parcels [between 2 and 4 hectares] account for roughly 20% of the total area of the GD. Agricultural parcels exceeding 4 hectares cover only 8% of the study area. The farmers have recently developed these large-sized parcels situated at the peripheries of the older ones. The study of agricultural parcels has revealed land fragmentation in the study area. Furthermore, information relating to parcel characteristics is crucial for studying farmland surfaces.

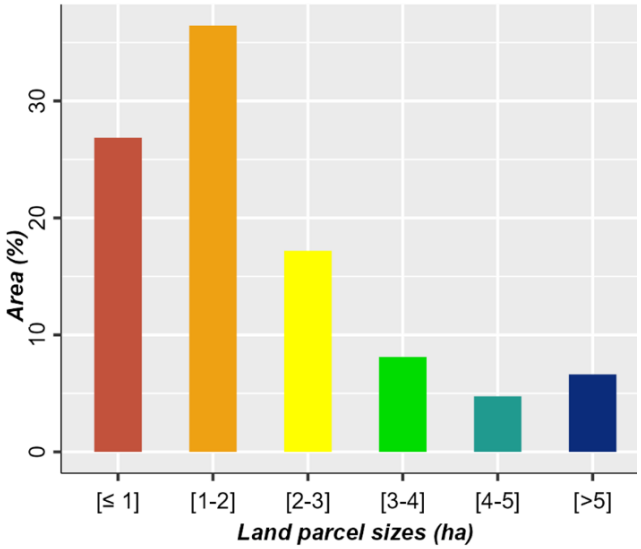

Figure 2. Distribution of agricultural parcels in the GD

2.2. Fieldwork

In August 2018, we conducted fieldwork to identify different land use (LU) classes. The types of irrigated crops in the study area were determined using a high-resolution map. The samples of irrigated crops observed and geolocated as polygons across the study area are compared with L8SI. This approach allowed us to precisely determine the characteristics of each type of crop and obtain detailed information about their spectral variations. Furthermore, the exhaustive characterization of irrigated crops in the GD, achieved through comparison between field-collected samples and those obtained from satellite imagery, facilitated their distinction from other LU classes (bare lands and buildings). Thus, we used the collected samples to monitor SR, classify the satellite image, and validate the obtained results. The crossing of field data with the false-color satellite image (Figure 3) led to the development of a LU typology in the GD in August 2018. At this time of the year, there is a distinct separability between the spectral signatures of irrigated crops and other LU classes. All irrigated crops exhibit specific and uniform responses, reflecting the coverage of active vegetation. In contrast, rainfed croplands post-harvest, bare lands (basaltic and limestone terrains), and habitats are visible in the satellite image and characterized by low spectral reflectance (SR).

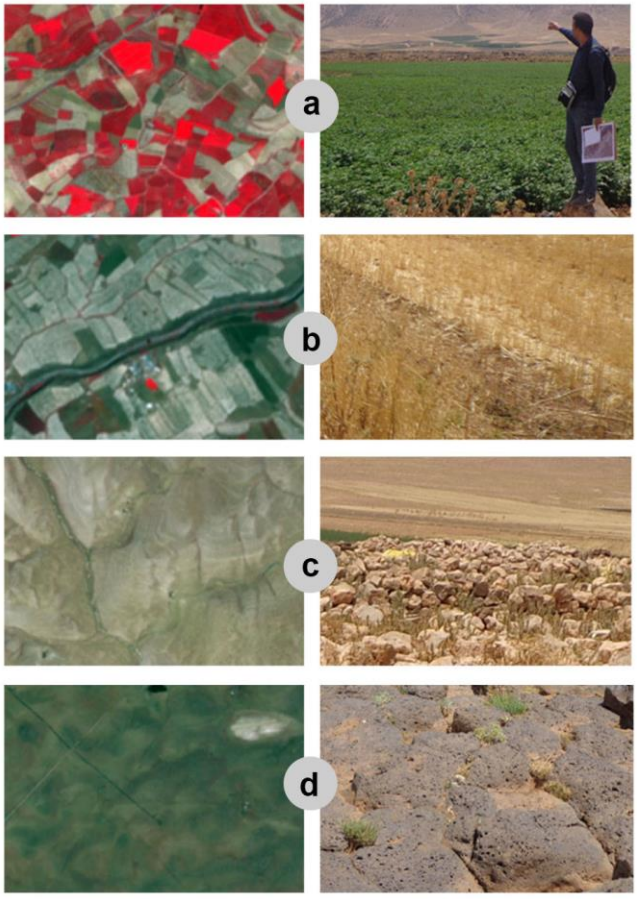

Figure 3. LU samples in the study area; a comparison between field and satellite image. a) irrigated crops (the light red color represents potatoes, while the dark red color corresponds to onions), b) rainfed croplands after harvest, c) basaltic terrains, d) limestone terrains.

2.3. Satellite data

In this study, Landsat 8 satellite images (L8SI) are the basis for monitoring SR. These images have been widely employed in research dedicated to mapping and tracking the evolution of land surfaces [27,45,46]. Landsat 8 OLI (Operational Land Imager) and TIRS (Thermal Infrared Sensor) images consist of nine spectral bands (1 to 7 and 9) with a spatial resolution of 30 meters. The panchromatic band (band 8), with a resolution of 15 meters, is used to enhance the spatial resolution of the spectral bands from 30 meters to 15 meters. The thermal bands (10 and 11) with a spatial resolution of 100 meters are practical for studying surface temperature. For SR monitoring, we applied preprocessing and processing to seven spectral bands. These mainly include bands in the visible (Blue, Green, and Red), Near Infrared (NIR), shortwave infrared 1 (SWIR 1), and shortwave infrared 2 (SWIR 2) ranges. The L8SI used in this study span from January to December 2018 (Table 1).

2.3.1. Preprocessing of Landsat 8 OLI images

RS data provided by the U.S. Geological Survey (USGS) require pre-processing to facilitate automatic classification and visual interpretation. Before their use, satellite images oblige radiometric and atmospheric pre-processing. Radiometric correction of satellite images allows the conversion of raw pixel values (digital numbers) into TOA (Top-of-Atmosphere) reflectance. Baghdadi and Zribi, [47] demonstrated that converting pixel values to reflectance is more effective for comparing satellite data. The conversion of pixel values to reflectance is performed according to the guidelines recommended by the USGS.

Table 1. Landsat 8 satellite images used in this study

Acquisition date: 2018	Sensor	Path/ Row	Spatial resolution
January 04	OLI	201/037	30 m
February 14	OLI	200/036	30 m
March 09	OLI	201/037	30 m
April 19	OLI	200/037	30 m
May 12	OLI	201/037	30 m
Jun 22	OLI	200/037	30 m
July 08	OLI	200/036	30 m
August 09	OLI	200/037	30 m
September 17	OLI	201/037	30 m
October 17	OLI	200/037	30 m
November 04	OLI	201/037	30 m
December 06	OLI	201/037	30 m

Data source: All data are available the on: https://earthexplorer.usgs.gov

The algorithm proposed by the USGS combines the spectral bands and the metadata file (MTL file) provided with the level 1 satellite image. The algorithm recommended by the USGS is integrated into the semi-automatic classification extension (SCP) developed by Congedo and installed in the QGIS software. The SCP plugin enables various functions such as downloading, pre-processing, and processing optical satellite images. This powerful package for QGIS [48] has been used in the domain of RS [49-52]. In parallel with radiometric correction, we performed atmospheric correction to eliminate atmospheric effects [53] based on the DOS 1 (Dark Object Subtract 1) model, which is an atmospheric model relying on image properties.

2.4. Classification Process

2.4.1. Classification Method

LU classification from satellite images relies on machine learning algorithms (Support Vector Machine, Random Forest, Maximum Likelihood, etc.) and the calculation of spectral indices (NDVI, EVI, SAVI, NDWI, etc.). The present work focuses on applying the Support Vector Machine (SVM) supervised classification algorithm commonly used by researchers [9,12,54-56]. This non-parametric algorithm has become very popular in remote sensing over the past decades due to its high accuracy in classification results, even when using a small number of training samples [12]. For the SVM classifier, the default kernel function is the Radial Basis Function (RBF) kernel. The RBF kernel is widely used [12,55,57,58] to capture complex nonlinear relationships between data points [58]. Thus, SVM with RBF kernel is one of the best classification algorithms [59]. The performance of the SVM with RBF kernel depends on the choice of parameters C and γ [60]. In general, if the values of C and gamma (γ) are small, the model tends to be underfitted, whereas if both parameters are high, it tends to be overfitted [61,62].

Hashim et al. [63] applied the non-optimized SVM parameters to map LU. In this study, we used the default RBF kernel for the SVM and the hyperparameters γ and C were set to 1.0 and scale, respectively (non-optimized C and γ parameters). The default hyperparameters C and γ were chosen in this work to avoid the risk of overfitting and underfitting the SVM model. Furthermore, discussing the significance of the values of C and γ is beyond the scope of this article. However, detailed information on the importance of the γ and C hyperparameters is available in [12,61].

2.4.2. Training samples and validation data

The SVM classification algorithm was used to identify LU classes using reference data collected in the field in 2018. The classification samples are distributed across the entire study area, with varying numbers from one class to another (Table 2). For validation purposes, we assigned 500 points to each LU class.

Table 2. Number of samples used for training

	Classes	Training samples (polygons)
Irrigated crops	Potatoes	24
	Onions	23
	Carrots	24
	Bare lands	25
	Buildings	23
Major LU classes	Irrigated areas	40
	Bare lands	26
	Buildings	23

The proposed methodology starts with fieldwork and progresses through multiple stages, culminating in the validation stage (Figure 4). The assessment of the classification results was based on samples collected in the field. The confusion matrix was calculated using the classification results and field data. Four evaluation metrics were derived from the confusion matrix: the F1 score, overall accuracy (OA), User Accuracy (UA), and Producer Accuracy (PA). These parameters, calculated using the R-statistical software (caret package), allow us to measure the agreement between the field-collected samples and those obtained from the classification. The accuracy assessment of classification in RS has been recognized as a valuable tool for assessing the reliability of obtained results [22,64,65]. Additionally, evaluating the accuracy of classified images against reference data enables the assessment of the classification algorithm's effectiveness.

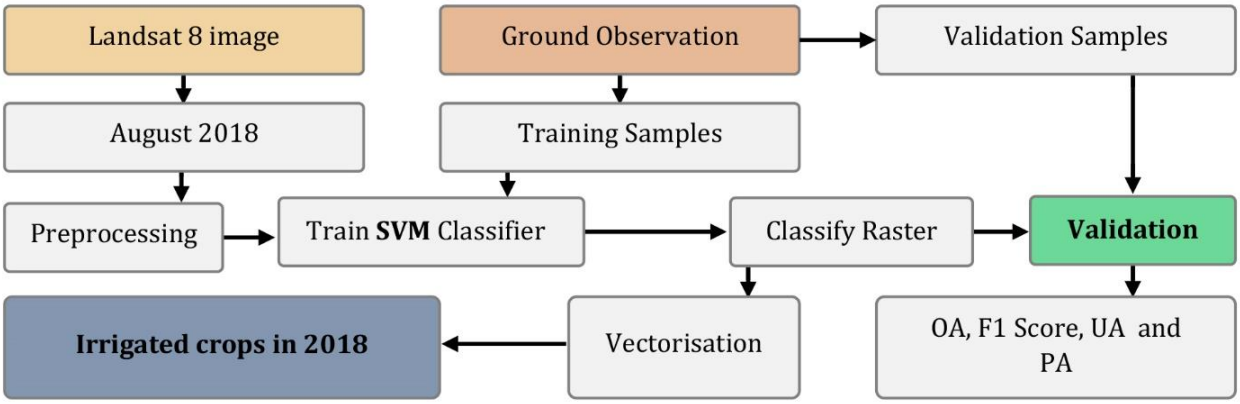

Figure 4. Flowchart of the proposed method in this study. OA: Overall Accuracy, UA: User Accuracy, PA: Producer Accuracy

3. Results and discussion

3.1. Determination of the favorable period for studying irrigated crops

To determine the suitable dates/periods for studying irrigated crops in the GD, we based on data collected during fieldwork in August 2018 and the analysis of SR from L8SI (from January to December 2018). Thus, SR was used to monitor the progression of phenological stages of irrigated crops. This approach reinforces the selection of a favorable period for studying this type of cultivation. Indeed, this study focuses on detecting irrigated crops as a crucial element for managing water resources.

3.1.1. Agricultural calendar

In the depression of Guigou, due to varied climatic conditions, farmers cultivate different types of crops throughout the year. These crops are categorized into two main types: rainfed crops and irrigated crops. Wheat, barley, oats, and rye are rainfed crops harvested between mid-May and mid-July, while irrigated crops such as potatoes, carrots, and onions are harvested from September to November. The sowing and harvesting dates of crops are presented in Figure 5, illustrating the agricultural calendar. This calendar depicts the main crops in the study area and their evolution throughout the year, from sowing to harvesting. It also serves to determine the legend of LU maps. The crop calendar illustrates the diversity of crops and their seasonal variations. For example, the phenological stage of wheat begins in mid-October (sowing) and extends until mid-May (harvesting). For potatoes, the phenological period starts from mid-April (sowing) to the end of August (harvesting). The agricultural calendar highlights that August is the most suitable month for detecting irrigated crops and April for rainfed crops. However, the study of rainfed crops falls outside the objectives of this article. Generally, the irrigation period in the study area begins in April, but the intensification of irrigation increases remarkably in July and August, characterized by a significant rise in temperature. Thus, this period coincides with the maturation stage of irrigated crops.

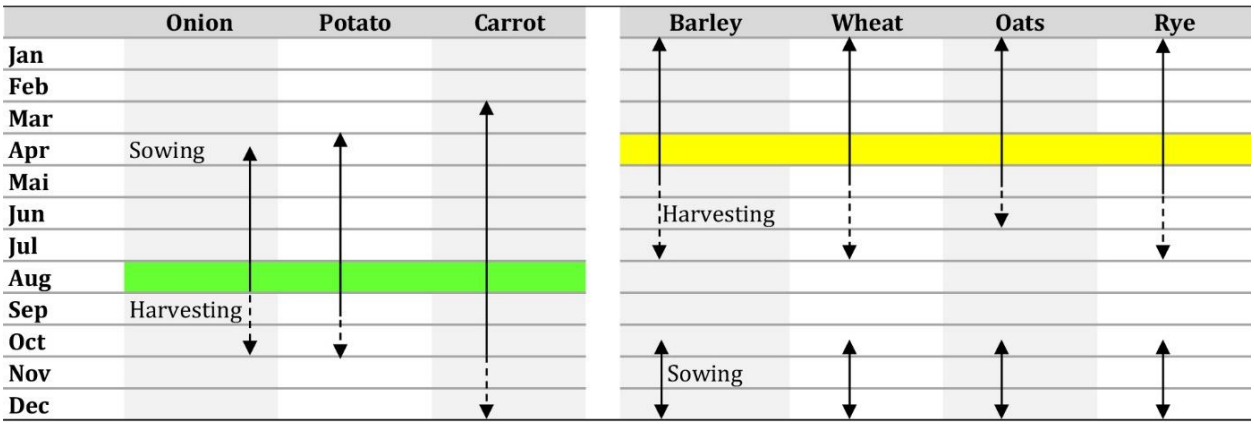

Figure 5. Agricultural calendar of irrigated and rainfed crops in the GD. In yellow: the favorable period for studying rainfed crops; in green: the optimal period for studying irrigated crops (fieldwork).

3.1.2. Spectral reflectance of irrigated crops

The analysis of SR has been the subject of several studies focusing on the spatiotemporal evolution of crops, forests, and wetlands [3,53,66,67]. In this work, the study of SR and field data allowed for identifying the favorable month for studying irrigated crops and selecting useful bands to distinguish LU classes from satellite images. The results obtained from the statistical analysis of SR (Figure 6) show its variation throughout the year and based on spectral bands. Indeed, August is the most acceptable for studying irrigated crops (potatoes, carrots, and onions). In August, the SR of irrigated crops showed the highest separability in the near-infrared (NIR). These results indicate that NIR is the most suitable for distinguishing changes in the

phenological stages of irrigated crops throughout the year. Although August is crucial for studying the three crops, September, October, and November are suitable for mapping carrots. During this period, carrots demonstrate high reflectance in the NIR.

Furthermore, there is a decrease in spectral signature in the bands of the visible spectrum (Blue, Green, and Red) and the bands of the Shortwave Infrared bands (SWIR 1 and SWIR 2). According to López-Serrano et al. [53], the spectral signature of vegetation shows high reflectance in the NIR. Monitoring the variations in SR throughout the year across different spectral bands allows distinguishing between irrigated crops and other LU classes. For example, bare lands consistently display a distinct spectral signature, while agricultural areas may exhibit seasonal variations linked to sowing and harvesting cycles. Hence, the analysis of SR has played a crucial role in determining the date and spectral band that allows the discrimination of irrigated agricultural lands from other LU classes. However, a detailed study of each type of yield (potatoes, onions, carrots) is a complex task due to the proximity of SR values in the NIR.

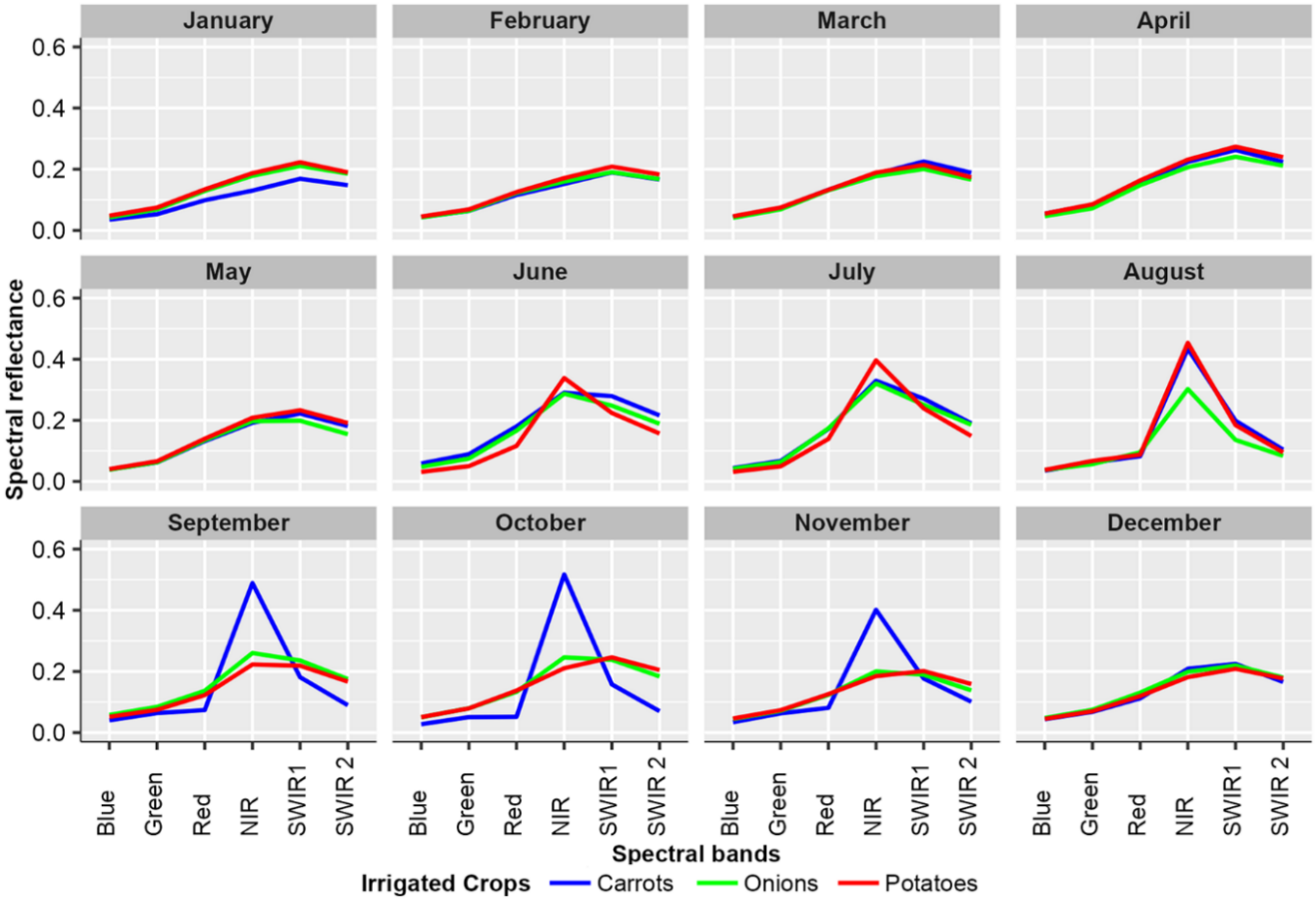

Figure 6. The spectral signature of irrigated crops during different phenological stages

Contrary to irrigated crops that exhibit a specific response in the NIR, the SR of bare land shows a notable decrease in spectral signature from June and demonstrates a similar response in the NIR. These values indicate limited or absent vegetation cover on these surfaces. In contrast, agricultural areas show seasonal variations, with peaks in the SR during cultivation and active vegetation periods. The combination of SR and fieldwork indicates that August is the most favorable month for distinguishing irrigated crops from other LU classes in the GD. Figure 7 depicts the distribution of SR in the NIR of irrigated crops. While there is clear separability between onions and other crops, the similarity in spectral signature values between potatoes and carrots makes the classification of the two types of crops very challenging. Additionally, the land fragmentation and the dominance of small-sized parcels (less than 2 hectares) that cover approximately 70% of the study area complicates the classification.

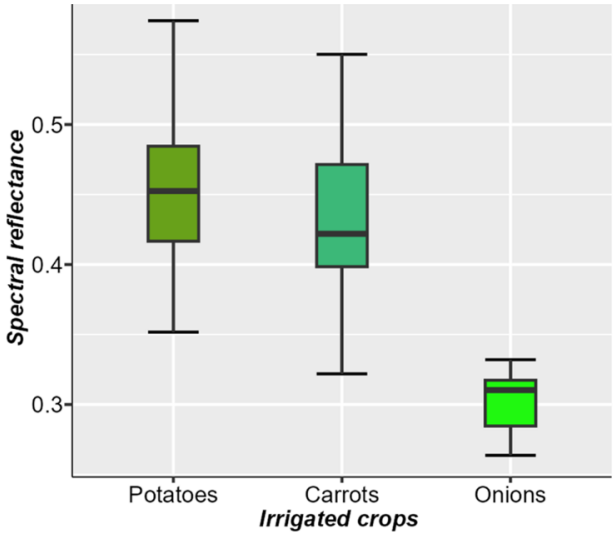

Figure 7. Illustration of the separability of irrigated crops in the GD in August 2018 using SR in the NIR

3. 2. Classification of irrigated crops

After selecting the satellite images suitable for studying irrigated crops in the GD, we conducted a supervised classification using samples collected from the field. The map (Figure 8) obtained from the classification of the satellite image of August 9, 2018, without clouds, illustrates the spatial distribution of irrigated crops. The observation of the map indicates a notable dominance of onions with an area of 3254 hectares, followed by potatoes covering an area of 456 hectares and carrots with 356 hectares. The remaining area is distributed between bare lands (basaltic and limestone terrains and rainfed croplands after harvest) and buildings.

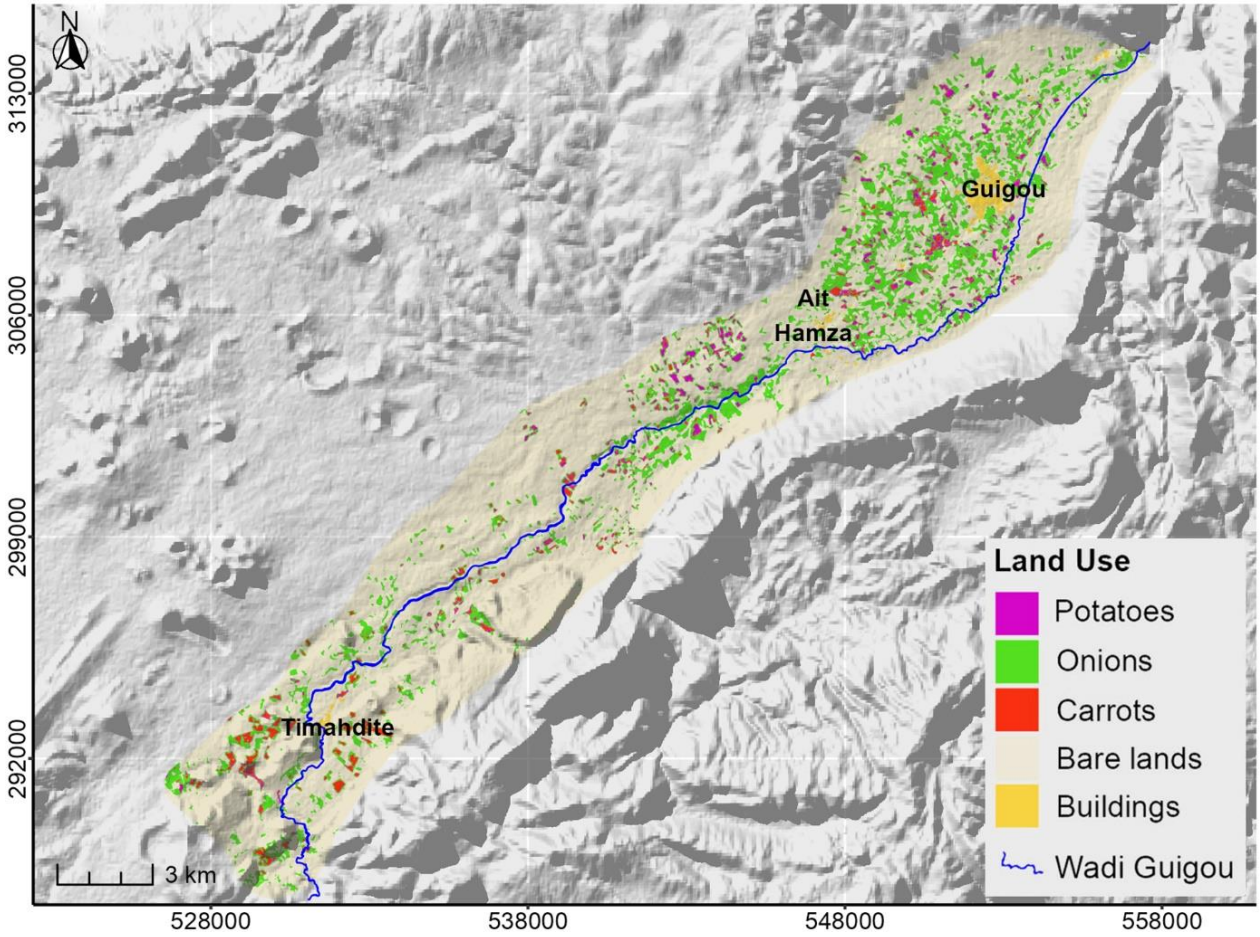

Figure 8. Mapping of irrigated crops, buildings and bare lands in the GD

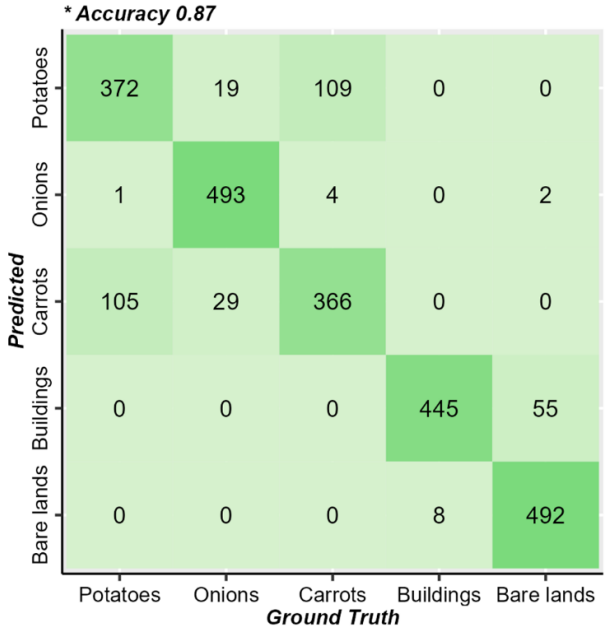

Figure 9. Confusion matrix of irrigated crops, buildings and bare lands

The classification results are subjected to a validation test based on field-derived data. The in-situ observations indicate that onions are well-classified. Potatoes and carrots present a low classification accuracy. Concurrently, we calculated the confusion matrix to assess the agreement between field samples and those of the classified image (Figure 9). The comparison of the two types of data indicates a strong agreement between the training data and the classification, with an accuracy of 0.87 (87%). Bare lands, habitats, and onions are well-classified with low classification errors. The F1 Score, Producer's Accuracy (PA), and User's Accuracy (UA) for these three classes exceed 0.88 (88%) (Table 3). Potatoes and carrots show lower accuracy, below 0.8 (80%), in contrast to other LU classes. The confusion matrix highlights that the two classes are not well-distinguished, with classification errors exceeding 20% of samples. The F1 Score, PA, and UA for the Potatoes and carrots are below 0.8 (80%). In the study area, the low classification accuracy of irrigated crops, particularly potatoes and carrots, is linked to the low separability of the SR of these two crop types. Therefore, the fragmentation of

agricultural parcels (parcels ≤ 1 and between 1 and 2 hectares constitute 72% of the study area) contributes to the reduction in classification accuracy. However, to correct classification errors, we can use data related to the variation in SR throughout the year. For potatoes, the decrease in SR values begins in September. For carrots, there is an increase in spectral reflectance values observed from September to November (Figure 6). The utilization of this data serves to distinguish potatoes from onions, consequently enhancing classification accuracy. Thus, this study proposes an alternative analysis scale based on the classification of major LU classes (irrigated surfaces, bare lands, and habitats).

Table 3. Per-class F1 Score, UA and PA of irrigated crops, buildings and bare lands

Classes	F1 Score	UA	PA
Potatoes	0.76	0.78	0.74
Onions	0 .95	0.91	0.99
Carrots	0.75	0,76	0.73
Buildings	0.93	0.98	0.89
Bare lands	0.94	0.90	0.98

The map (Figure 10) depicts the classification results of major LU classes in the GD. Three principal classes were distinguished: irrigated surfaces, bare lands, and habitats. The comparison of the classified map with in situ observations reveals a very high classification accuracy. Thus, the statistical validation (Figure 11) indicates a strong correspondence between the classified image and the ground truth, with an overall accuracy of 0.97 (97%). The samples used in the classification indicate that the three LU classes (irrigated surfaces, bare lands, and buildings) are well classified. The errors depicted in Figure 11 are low, with 40 samples for bare lands and 12 samples for buildings. The irrigated agricultural surfaces demonstrate high separability compared to other LU classes. The F1 Score, PA, and UA exceed 0.9 for all three classes (Table 4), but irrigated areas indicate the highest precision (0.99, 1, and 0.99 for F1 Score, PA, and UA, respectively).

The validation of the maps (Figures 8 and 10), derived from the analysis of the satellite image taken on August 9, 2018, reveals that the classification accuracy varies among different LU classes. Initially, we classified crop types and other LU classes in the study area. The results indicate a good classification accuracy for all classes, with an accuracy of 0.87 (87%). These metrics demonstrate the reliability of the classification process, demonstrating a high level of agreement between the predicted land use classes and the ground truth data. However, potatoes and carrots exhibit a precision lower than 0.8 (80%). The F1 Score, PA, and UA of crops illustrate this finding. The confusion between potatoes and carrots is related to the similarity of SR values for the crops and the dominance of small-sized parcels.

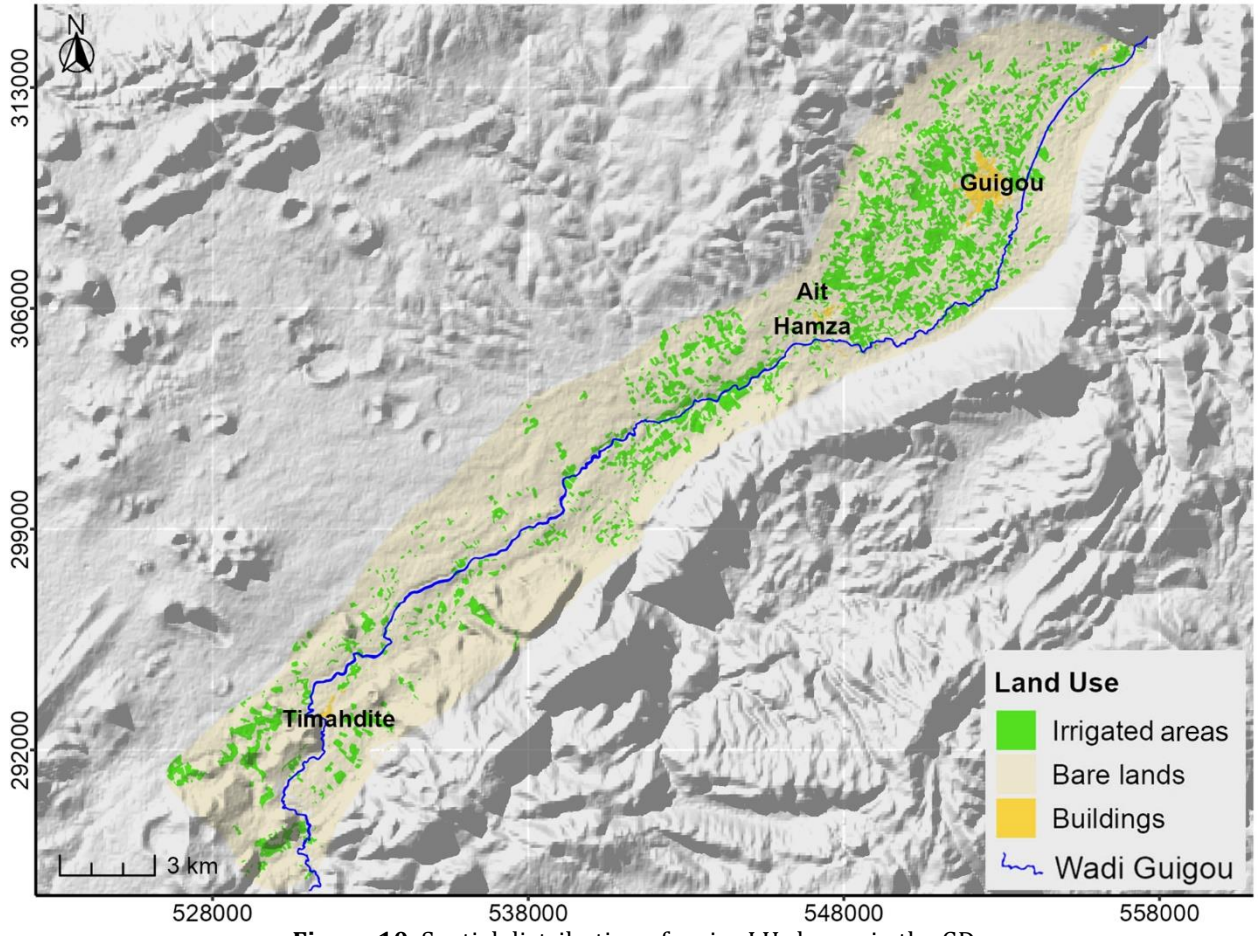

Figure 10. Spatial distribution of major LU classes in the GD

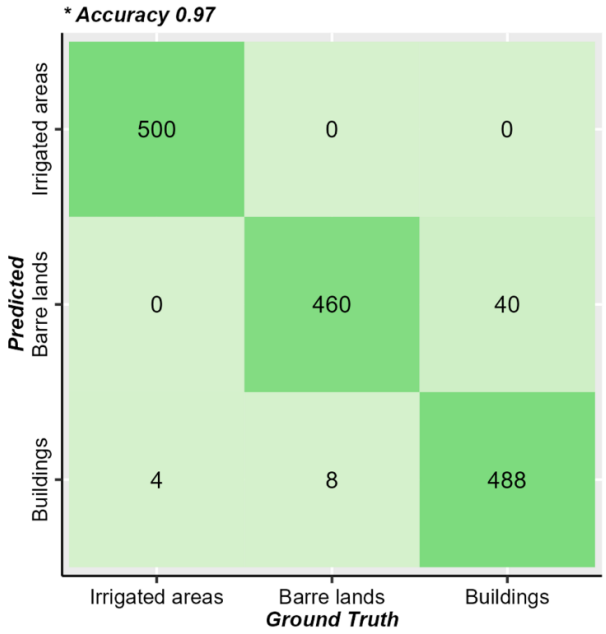

Figure 11. Confusion matrix of major LU classes

Table 4. Per-class F1 Score, UA and PA of major LU classes

Classes	F1 Score	UA	PA
Irrigated areas	0.99	0.99	1.00
Bare lands	0.95	0.98	0.92
Buildings	0.95	0.92	0.98

To improve the classification accuracy, processing an image from other months characterized by an increase in SR (September, October, and November) can be used, particularly for carrots. Secondly, the major LU classes were classified. The results obtained indicate a high classification accuracy. Based on the level of classification precision, we observe that the combination of SR and fieldwork provides a high potential for distinguishing irrigated agricultural lands from other LU classes. Overall, the high values of classification accuracy indicators (FI Score, PA, UA, and ground truth) demonstrate the effectiveness and reliability of the methodology, which relies on data from multiple sources. The methodological steps developed in this study provide a robust approach that authors in various regions can employ to identify optimal periods for studying irrigated agricultural surfaces.

3.3. Discussion

The study focuses on determining favorable periods for studying irrigated crops in the GD using fieldwork data and the analysis of SR from L8SI. The SR analysis and field data indicate that August is the most favorable month for identifying irrigated crops in the GD. The classification results of the different crop types show a significant confusion between potatoes and carrots. However, the classification of major LU classes demonstrates high accuracy, with an accuracy exceeding 0.95 (95%). Despite lower precision in classifying individual crops, the proposed methodology proves reliable for identifying optimal periods for studying irrigated areas.

While satellite images provide a valuable resource for studying land surfaces, several challenges are associated with processing this data. The analysis of satellite images to extract information requires extensive fieldwork. This fieldwork is crucial to identify different LU classes and gather training samples for the classification and validation processes. For recent satellite images, fieldwork provides essential data on LU. However, classifying older images for a diachronic study demands a better understanding of the spectral characteristics of different LU classes based on recent satellite images. However, extracting data from satellite images requires monitoring the variation in SR throughout the year to select the favorable period and spectral bands for studying different LU classes. The information derived from analyzing SR can used to correct classification errors.

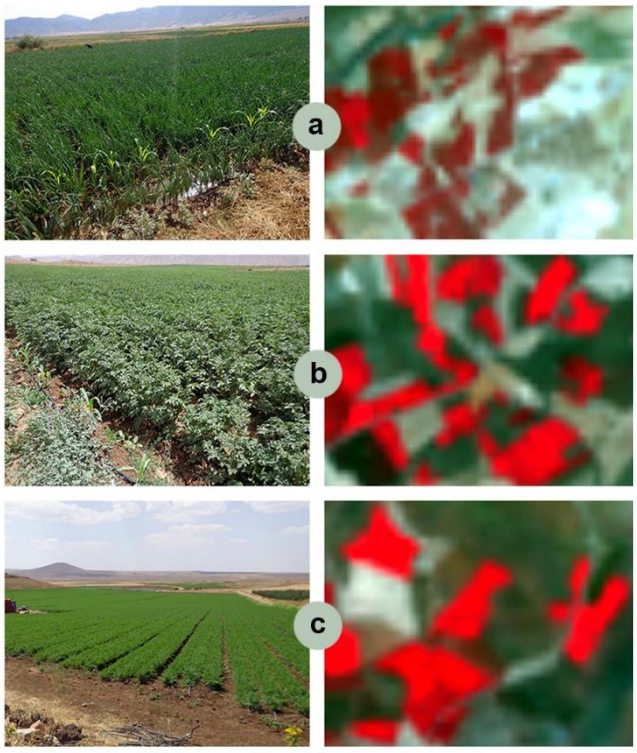

Figure 12. Samples of irrigated crops in the GD; a comparison between in situ data and Landsat 8 satellite image (August 9, 2018) in false color. a) Onions, b) Potatoes, c) Carrots. The light red color represents potatoes and carrots, while the dark red color corresponds to onions.

The proximity of SR values in the NIR between crop types, such as potatoes and carrots, presents a challenge for separability (Figure 12). This proximity makes it difficult to distinguish between these crop types with high precision. To address this problem, we proposed considering temporal variations in SR throughout the year. Although August is the favorable month for mapping irrigated crops, the study suggests the potential use of images from other months, such as September, October, and November, to improve classification accuracy, especially for carrots. Thus, the fragmentation of agricultural parcels can contribute to a reduction in classification precision. In the GD, small-sized parcels, constituting approximately 72% of agricultural land,

contribute to reduced classification accuracy and complicate the precise identification of irrigated crops. While this work focuses explicitly on irrigated crops, the methodology developed can be used to study rainfed crops in diverse environmental conditions. Since the current study concentrates on irrigated crops, future research could include a detailed analysis of irrigated and rainfed crops in areas marked by the dominance of small-sized parcels and regions characterized by large-sized parcels. Additionally, comparing supervised classification algorithms (Support Vector Machine, Random Forest, Maximum Likelihood) to assess the accuracy of each algorithm in separating irrigated and rainfed crops from other LU classes would be an intriguing avenue for further research.

4. Conclusion

The studies focused on satellite image processing have recorded a remarkable increase in recent decades, reflecting the growing importance and utilization of such data in various fields. The multiplication of publications has been facilitated by free access to multi-source images (Landsat, MODIS, and Sentinel), the development of machine learning algorithms, and the emergence of powerful image processing tools. The studies carried out in this context are numerous, and the results obtained in various countries around the globe demonstrate the high potential of optical satellite images in mapping, monitoring, and quantifying LU at different scales. In this regard, RS provides valuable data to address specific environmental problems, especially in managing natural resources (water resources, forests, etc.). However, extracting information from satellite images requires following a robust methodology. In several locations across the globe, the processing of satellite images for extracting LU classes has been based on the analysis of SR. The results obtained in different locations worldwide indicate that these criteria represent a high potential for accurately studying the Earth's surface. Amani et al. [66] demonstrated the capacity of SR in detecting wetland areas in Canada. The optimal selection of spectral bands for Investigating these areas was illustrated by the high level of accuracy in the classification results, with an average overall accuracy of 86%. In northern China, the employment of spectral and temporal features of satellite images by Wang et al. [68] worked perfectly to map and distinguish forest species, with an accuracy exceeding 90%.

This study proposes an approach using fieldwork and SR analysis to identify optimal dates and bands for studying irrigated crops in the GD. SR analysis highlighted that the NIR band is the most suitable for distinguishing irrigated crops from other LU classes. Consequently, we observed that August is optimal for studying irrigated crops based on field data and SR. The results obtained from the processing of satellite images indicate that the classification accuracy varies depending on the legend selected (irrigated crops and major LU classes). The high or low agreement between in situ data and classification is linked to the separability of the SR of crops, the size of agricultural parcels, and the criteria used for selecting the legend. This study has demonstrated that the methodology followed has resulted in the mapping of irrigated crops in the GD. In parallel with the criteria chosen in this study for detecting irrigated crops, incorporating vegetation indices such as NDVI and EVI can improve the classification accuracy of satellite images. Finally, the quantification of irrigated crops is an essential element for efficient water resources management.

Acknowledgments

The authors wish to express their deep gratitude to the U.S. Geological Survey (USGS) for providing the Landsat satellite images free of charge. We would also like to extend our sincere thanks to the reviewers for their valuable insights and constructive feedback, which have significantly contributed to improving the manuscript.

Author contributions

Abdelaziz El-Bouhali: Conceptualization, Methodology, Software, Data analysis, Writing – original draft. **Mhamed Amyay**: Supervision, Writing – review & editing, Validation. **Khadija El Ouazani Ech-Chahdi**: Methodology, Data analysis, Writing - Review & editing.

Conflicts of interest

The authors declare no conflicts of interest.

References

1. Alexandridis, T. K., Zalidis, G. C., & Silleos, N. G. (2008). Mapping irrigated area in Mediterranean basins using low cost satellite Earth Observation. Computers and Electronics in Agriculture, 64, 93–103. https://doi.org/10.1016/j. compag.2008.04.001
2. Xie, Y., & Lark, T. J. (2021). Mapping annual irrigation from Landsat imagery and environmental variables across the conterminous United States. Remote Sensing of Environment, 260, 112445. https://doi.org/10.1016/j.rse.2021.112445
3. Ouzemou, J. E., El-Harti, A., Lhissou, R., El-Moujahid, A., Bouch, N., El-Ouazzani, R., Bachaoui, E., & El Ghmari, A. (2018). Crop type mapping from pansharpened Landsat 8 NDVI data: A case of a highly fragmented and intensive agricultural system. Remote Sensing Applications: Society and Environment, 11, 94–103. doi: https://doi.org/10.1016/j.rsase.2018.05.002
4. Shema, R. A., & Lanhai, L. (2024). A geo-spatial analysis of precipitation distribution and its impacts on vegetation in Rwanda. Advanced GIS, 4(1), 24–30. https://publish.mersin.edu.tr/index.php/agis/article/view/1362
5. Guliyev, İsmail., & Hüseynov, R. (2024). Comparative character and monitoring of some parameters of the soil and vegetation by remote sensing in the zone of Zangilan. Advanced Remote Sensing, 4(1), 28–35. https://publish.mersin.edu.tr/index.php/arsej/article/view/1079
6. Xu, L., Herold, M., Tsendbazar, N. E., Masiliunas, D., Li, L., Lesiv, M., Fritz, S., & Verbesselt, J. (2022). Time series analysis for global land cover change monitoring: A comparison across sensors. Remote

Sensing of Environment, 271. 112905. https://doi.org/10.1016/j.rse.2022.112905
7. Mountrakis, G., Im, J., & Ogole, C. (2011). Support vector machines in remote sensing: A review. ISPRS Journal of Photogrammetry and Remote Sensing, 66, 247–259. https://doi.org/10.1016/j.isprsjprs.2010.11.001
8. Htitiou, A., Boudhar, A., Lebrini, Y., Hadria, R., Lionboui, H., Elmansouri, L., Tychon, B., & Benabdelouahab, T. (2019). The Performance of Random Forest Classification Based on Phenological Metrics Derived from Sentinel-2 and Landsat 8 to Map Crop Cover in an Irrigated Semi-arid Region. Remote Sens Earth Syst. Sci., 2, 208–224. https://doi.org/10.1007/s41976-019-00023-9
9. Ahmadi, K., Kalantar, B., Saeidi, V., Harandi, E. K. G., Janizadeh, S., & Ueda, N. (2020). Comparison of machine learning methods for mapping the stand characteristics of temperate forests using multi-spectral sentinel-2 data. Remote Sensing, 12, 3019. doi: https://doi.org/10.3390/rs12183019
10. Pervez, Md. S., Budde, M., & James Rowland, J. (2014). Mapping irrigated areas in Afghanistan over the past decade using MODIS NDVI. Remote Sensing of Environment, 149, 155–165. https://doi.org/10.1016/j.rse.2014.04.008
11. Şenol, H. İ., Kaya, Y., Yiğit, A. Y., & Yakar, M. (2024). Extraction and geospatial analysis of the Hersek Lagoon shoreline with Sentinel-2 satellite data. Survey Review, 56(397), 367-382.
12. Zheng, B., Myint, S. W., Thenkabail, P. S., & Aggarwal, R. M. (2015). A support vector machine to identify irrigated crop types using time-series Landsat NDVI data. International Journal of Applied Earth Observation and Geoinformation, 34, 103–112. https://doi.org/10.1016/j.jag.2014.07.002
13. Rhyma, P. P., Norizah, K., Hamdan, O., Faridah-Hanum, I., & Zulfa, A. W. (2020). Integration of normalised different vegetation index and Soil Adjusted Vegetation Index for mangrove vegetation delineation. Remote Sensing Applications. Society and Environment, 17, 100280. https://doi.org/10.1016/j.rsase.2019.100280
14. Eid, A. N. M., Olatubara, C. O., Ewemoje, T. A., Talaat El-Hennawy, M., & Farouk, H. (2020). Inland wetland time-series digital change detection based on SAVI and NDWI indecies: Wadi El-Rayan lakes, Egypt. Remote Sensing Applications: Society and Environment, 19, 100347. https://doi.org/10.1016/j.rsase.2020.100347
15. Dijk, D. V., Shoaie, S., Leeuwen, T. V., & Veraverbeke, S. (2021). Spectral signature analysis of false positive burned area detection from agricultural harvests using Sentinel-2 data. International Journal of Applied Earth Observations and Geoinformation, 97, 102296. https://doi.org/10.1016/j.jag.2021.102296
16. Azevedo, R. P., Dallacort, R., Boechat, G. L., Teodoro, P. E., Teodoro, L. P. R., & et al. (2023). Remotely sensed imagery and machine learning for mapping of sesame crop in the Brazilian Midwest. Remote Sensing Applications: Society and Environment, 32, 101018. https://doi.org/10.1016/j.rsase.2023.101018
17. Vogels, M. F. A., de Jong, S. M., Sterk, G., & Addink, E. A. (2019). Mapping irrigated agriculture in complex landscapes using SPOT6 imagery and object-based image analysis – A case study in the Central Rift Valley, Ethiopia. International Journal of Applied Earth Observation and Geoinformation, 75, 118–129. https://doi.org/10.1016/j.jag.2018.07.019
18. Mao, D., Wang, Z., Du, B., Li, L., Tian, Y., Jia, M., Zeng, Y., Song, K., Jiang, M., & Wang, Y. (2020). National wetland mapping in China: A new product resulting from object based and hierarchical classification of Landsat 8 OLI images. ISPRS Journal of Photogrammetry and Remote Sensing, 164, 11–25. https://doi.org/10.1016/j.jag.2014.01.020
19. Maselli, F., Battista, P., Chiesi, M., Rapi, B., Angeli, L., Fibbi, L., Magno, R., & Gozzini, B. (2020). Use of Sentinel-2 MSI data to monitor crop irrigation in Mediterranean areas. International Journal of Applied Earth Observation and Geoinformation, 93, 102216. https://doi.org/10.1016/j.jag.2020.102216
20. Siraj, M., Mahmood, S., & Habib, W. (2023). Geo-spatial assessment of land cover change in District Dera Ismail Khan, Khyber Pakhtunkhwa, Pakistan. Advanced Remote Sensing, 3(1), 1–9. https://publish.mersin.edu.tr/index.php/arsej/article/view/686
21. Benbahrıa, Z., Sebari, I., Hajji, H., Smiej, M. F. (2021). Intelligent mapping of irrigated areas from Landsat 8 images using transfer learning. International Journal of Engineering and Geosciences, 6(1), 40-50. https://doi.org/10.26833/ijeg.681312
22. Zurqani, H. A., Allen, J. S., Post, C. J., Pellett, C. A., & Walker, T. C. (2021). Mapping and quantifying agricultural irrigation in heterogeneous landscapes using Google Earth Engine. Remote Sensing Applications: Society and Environment, 23, 100590. https://doi.org/10.1016/j.rsase.2021.100590
23. Gull, A., & Mahmood, S. (2022). Spatio-temporal analysis and trend prediction of land cover changes using markov chain model in Islamabad, Pakistan. Advanced GIS, 2(2), 52–61. https://publish.mersin.edu.tr/index.php/agis/article/view/679
24. Shafiq, M., & Mahmood, S. (2022). Spatial assessment of forest cover change in Azad Kashmir, Pakistan. Advanced GIS, 2(2), 62–69. https://publish.mersin.edu.tr/index.php/agis/article/view/689
25. Ozdogan, M., Yang, Y., Allez, G., & Cervantes, C. (2010). Remote Sensing of Irrigated Agriculture: Opportunities and Challenges. Remote Sensing, 2, 2274–2304. https://doi.org/10.3390/rs2092274
26. Marino, S. (2023). Understanding the spatio-temporal behavior of crop yield, yield components and weed pressure using time series Sentinel-2-data in an organic farming system. European Journal of Agronomy, 145, 126785. https://doi.org/10.1016/j.eja.2023.126785
27. Bian, J., Lia, A., Leia, G., Zhanga, Z., & Nana, X. (2020). Global high-resolution mountain green cover index mapping based on Landsat images and Google Earth Engine. ISPRS Journal of Photogrammetry and

Remote Sensing, 162, 63–76. https://doi.org/10.1016/j.isprsjprs.2020.02.011
28. Dutrieux, L. P., Jakovac, C. C., Latifah, S. H., & Kooistra. L. (2016). Reconstructing land use history from Landsat time-series Case study of a swidden agriculture system in Brazil. International Journal of Applied Earth Observation and Geoinformation, 47, 112–124. http://dx.doi.org/10.1016/j.jag.2015.11.018
29. Belgiu, M., & Csillik, O. (2018). Sentinel-2 cropland mapping using pixel-based and object-based timeweighted dynamic time warping analysis. Remote Sensing of Environment, 204, 509–523. http://dx.doi.org/10.1016/j.rse.2017.10.005
30. Czekajlo, A., Coops, N. C., Wulder, M. A., Hermosilla, T., White, J. C., & Van Den Bosch, M. (2021). Mapping dynamic peri-urban land use transitions across Canada using Landsat time series: Spatial and temporal trends and associations with socio-demographic factors. Computers, Environment and Urban Systems, 88, 101653. https://doi.org/10.1016/j.compenvurbsys.2021.101653
31. Delgado-Artés, R., Garófano-Gómez, V., Oliver-Villanueva, J. V., & Rojas-Briales, E. (2022). Land use/cover change analysis in the Mediterranean region: a regional case study of forest evolution in Castelló (Spain) over 50 years. Land Use Policy, 114, 105967. https://doi.org/10.1016/j.landusepol.2021.105967
32. GCOS. (2016). The global observing system for climate: implementation needs. Global Climate Observing System implementation plan.
33. Lemmen, C. (2009). World distribution of land cover changes during Pre- and Protohistoric Times and estimation of induced carbon releases. Géomorphologie : relief, processus, environnement, 15(4), 303-312. https://doi.org/10.4000/geomorphologie.7756
34. Morrison, K. D., Hammer, E., Boles, O., Madella, M., Whitehouse, N., Gaillard, M. J., & et al. (2021). Mapping past human land use using archaeological data: A new classification for global land use synthesis and data harmonization. PLoS ONE, 16(4), e0246662. https://doi.org/10.1371/journal.,pone.0246662
35. Schaldach, R., Koch, J., der Beek, T. A., Kynast, E., & Flörke, M. (2012). Current and future irrigation water requirements in pan-Europe: An integrated analysis of socio-economic and climate scenarios. Global and Planetary Change, 94–95, 33–45. doi:10.1016/j.gloplacha.2012.06.004
36. Pageot, Y., Baup, F., Inglada, J., Baghdadi, N., & Demarez, V. (2020). Detection of irrigated and rainfed crops in temperate areas using sentinel-1 and sentinel-2 time series. Remote Sensing, 12, 3044. doi :http://dx.doi.org/10.3390/rs12183044
37. Zeryouhi, I. (1977). Le Moyen Atlas Plisse, In Ressources en Eau du Maroc Tome 3 Domaines atlasique et sud atlasique. Ed. Service géologique du Maroc, Rabat, 66-84.
38. Akdim, B., Sabaoui, A., Amyay, A., Laaouane, M., Gille, E., & Obda, Kh. (2011). Influences hydro karstiques du système sourcier Aïn Sebou-Timedrine-Ouamender sur l'hydrologie de l'oued Sebou (Moyen Atlas, Maroc). Zeitschrift für Geomorphologie, 56(2), 165-181. doi: 10.1127/0372-8854/2011/0063
39. Yakar, M., & Dogan, Y. (2019). 3D Reconstruction of Residential Areas with SfM Photogrammetry. In Advances in Remote Sensing and Geo Informatics Applications: Proceedings of the 1st Springer Conference of the Arabian Journal of Geosciences (CAJG-1), Tunisia 2018 (pp. 73-75). Springer International Publishing.
40. Amyay, M., Laaouane, M., & Akdim, B. (2000). La pression anthropique sur les ressources en eau souterraine dans le Moyen Atlas. Exemple de la dépression d'Afourgagh. Mosella, 3-4, 341-351.
41. Loubignac, V. (1938). Le régime des eaux, le nantissement et la prescription chez les Ait Youssi du Guigou. Hesperis, XXV, 251-264.
42. El-Bouhali, A. (2023). L'évolution des surfaces irriguées et leur impact sur les ressources en eau dans le contexte climatique actuel au Moyen Atlas tabulaire. [Thèse de doctorat, Université Sidi Mohamed Ben Abdellah – Fès].
43. El-Bouhali, A., Amyay, M., & El Ouazani Ech-Chahdi, K. (2024). Combined impact of drought and land use changes on water resources in the Tabular Middle Atlas, Morocco. Revista de Estudios Andaluces (48), 202-220. https://dx.doi.org/10.12795/rea.2024.i48.10
44. El-Bouhali, A., Amyay, M., & El Ouazani Ech-Chahdi, K. (2024). Recent variations of water area in the Tabular Middle Atlas lakes, Morocco. IOP Conf. Series: Earth and Environmental Science, 1398, 012012. https://doi.org/10.1088/1755-1315/1398/1/012012
45. El Jazouli, A., Barakat, A., Khellouk, R., Rais, J., & El Baghdadi, M. (2019). Remote sensing and GIS techniques for prediction of land use land cover change effects on soil erosion in the high basin of the Oum Er Rbia River (Morocco). Remote Sensing Applications: Society and Environment, 13, 361–374. https://doi.org/10.1016/j.rsase.2018.12.004
46. Bayo, B., Habib, W., & Mahmood, S. (2022). Spatio-temporal assessment of mangrove cover in the Gambia using combined mangrove recognition index. Advanced Remote Sensing, 2(2), 74–84. https://publish.mersin.edu.tr/index.php/arsej/article/view/685
47. Baghdadi, N., & Zribi, M. (2017). Observation des surfaces continentales par télédétection optique techniques et méthodes. Edition, ISTE Ltd 1.
48. Correia, R., Duarte, L., Teodoro, A. C., & Monteiro, A. (2018). Processing Image to Geographical Information Systems (PI2GIS)-A Learning Tool for QGIS. Educ. Sci., 8, 83. doi:10.3390/educsci8020083
49. Obodai, J., Adjei, K. A., Odai, S. N., & Lumor, M. (2019). Land use/land cover dynamics using landsat data in a gold mining basin-the Ankobra, Ghana. Remote Sensing Applications: Society and Environment, 13, 247–256. https://doi.org/10.1016/j.rsase.2018.10.007

50. Yılmaz, H. M., Yakar, M., Mutluoğlu, O., & Yıldız, F. (2004). Selection of the most suitable sizes of ground control points in the satellite images. International Society for Photogrammetry and Remote Sensing.
51. Congedo, L. (2021). Semi-Automatic Classification Plugin: A Python tool for the download and processing of remote sensing images in QGIS. Journal of Open Source Software, 6(64), 3172. https://doi.org/10.21105/joss.03172
52. Abdul Azeez, S., Gnanappazham, L., Muraleedharan, K. R., Revichandran, C., John, S., Seena, G., & Jubin Thomas, T. (2022). Multi-decadal changes of mangrove forest and its response to the tidal dynamics of thane creek, Mumbai. Journal of Sea Research, 180, 102162. https://doi.org/10.1016/j.seares.2021.102162
53. López-Serrano, P. M., Corral-Rivas, J. J., Díaz-Varela, R. A., Álvarez-González, J. G., & López-Sánchez, C. A. (2016). Evaluation of Radiometric and Atmospheric Correction Algorithms for Aboveground Forest Biomass Estimation Using Landsat 5 TM Data. Remote Sensing, 8(5), 369. https://doi.org/10.3390/rs8050369
54. Rana, V. K., & Venkata-Suryanarayana, T. M. (2020). Performance evaluation of MLE, RF and SVM classifcation algorithms for watershed scale land use/land cover mapping using sentinel 2 bands. Remote Sensing Applications: Society and Environment, 19, 100351. doi:https: //doi.org/10.1016/j.rsase.2020.100351
55. Avci, C., Budak, M., Yağmur, N., & Balçik, F. B. (2023). Comparison between random forest and support vector machine algorithms for LULC classification. International Journal of Engineering and Geosciences, 8(1), 1-10. https://doi.org/10.26833/ijeg.987605
56. El-Bouhali, A., Amyay, M., & El Ouazani Ech-Chahdi, K. (2024). Changes in water surface area of the Middle Atlas-Morocco lakes: A response to climate and human effects. International Journal of Engineering and Geosciences, 9(2), 221-232. https://doi.org/10.26833/ijeg.1391957
57. Ghassemi, B., Dujakovic, A., Żółtak, M., Immitzer, M., Atzberger, C., & Vuolo, F. (2022). Designing a European-Wide Crop Type Mapping Approach Based on Machine Learning Algorithms Using LUCAS Field Survey and Sentinel-2 Data. Remote Sensing, 14, 541. https://doi.org/10.3390/rs14030541
58. Abd El-Hamid, H.T., Alshehri, F., El-Zeiny, A.M., & Nour-Eldin, H. (2023). Remote sensing and statistical analyses for exploration and prediction of soil salinity in a vulnerable area to seawater intrusion. Marine Pollution Bulletin, 187, 114555. https://doi.org/10.1016/j.marpolbul.2022.114555
59. Prajapati, G. L., & Patle, A. (2010). On Performing Classification Using SVM with Radial Basis and Polynomial Kernel Functions. 3rd International Conference on Emerging Trends in Engineering and Technology, Goa, India, 512-515. https://doi.org/10.1109/icetet.2010.134
60. Wainer, J., & Fonseca, P. (2021). How to tune the RBF SVM hyperparameters? An empirical evaluation of 18 search algorithms. Artificial Intelligence Review, 54, 4771–4797. https://doi.org/10.1007/s10462-021-10011-5
61. Potić, l, Srdić, Z.; Vakanjac, B., Bakrač, S., Đorđević, D., Banković, R., & Jovanović, J.M. (2023). Improving Forest Detection Using Machine Learning and Remote Sensing: A Case Study in Southeastern Serbia. Applied Sciences, 13, 8289. https://doi.org/10.3390/app13148289
62. Fang, P., Zhang, X., Wei, P., Wang, Y., Zhang, H., Liu, F., & Zhao, J. (2020). The Classification Performance and Mechanism of Machine Learning Algorithms in Winter Wheat Mapping Using Sentinel-2 10 m Resolution Imagery. Applied Sciences, 10(5), 5075. https://doi.org/10.3390/app10155075
63. Alonso-Sarría, F., Valdivieso-Ros, C., & Gomariz-Castillo, F. (2024). Analysis of the hyperparameter optimisation of four machine learning satellite imagery classification methods. Computational Geosciences 28, 551–571. https://doi.org/10.1007/s10596-024-10285-y
64. Hashim, F., Dibs, H., & Jaber, H.S. (2021). Applying Support Vector Machine Algorithm on Multispectral Remotely sensed satellite image for Geospatial Analysis. Journal of Physics: Conference Series, 1963, 012110. https://doi.org/10.1088/1742-6596/1963/1/012110
65. Meer, M. S., & Mishra, A. K. (2020). Remote sensing application for exploring changes in land use and land cover over a district in Northern India. Journal of the Indian Society of Remote Sensing, 48, 525-534. https://doi.org/10.1007/s12524-019-01095-2
66. Amani, M., Salehi, B., Mahdavi, S., & Brisco, B. (2018). Spectral analysis of wetlands using multi-source optical satellite imagery. ISPRS Journal of Photogrammetry and Remote Sensing, 144, 119–136. https://doi.org/10.1016/j.isprsjprs.2018.07.005
67. El-Hendawy, S. E., Al-Suhaibani, N. A., Hassan, W. M., Dewir, Y. H., Elsayed, S., Al Ashkar, I., Abdella, K. A., & Schmidhalter, U. (2019). Evaluation of wavelengths and spectral reflectance indices for high-throughput assessment of growth, water relations and ion contents of wheat irrigated with saline water. Agricultural Water Management, 212, 358–377. https://doi.org/10.1016/j.agwat.2018.09.009
68. Wang, M., Zheng, Y., Huang, C., Meng, R., Pang, Y., & et al. (2022). Assessing Landsat-8 and Sentinel-2 spectral-temporal features for mapping tree species of northern plantation forests in Heilongjiang Province, China. Forest Ecosystems, 9, 100032. https://doi.org/10.1016/j.fecs.2022.100032